

Diastereomeric Δ -1,4,7,10-Tetrakis((*R*)-2-hydroxy-2-phenylethyl)-1,4,7,10-tetraazacyclododecane and Its Alkali-Metal Complex Ions. A Potentiometric Titration, Nuclear Magnetic Resonance, and Molecular Orbital Study

Sonya L. Whitbread,[†] Peter Valente,[‡] Mark A. Buntine,[†] Philip Clements,[†] Stephen F. Lincoln,^{*,†} and Kevin P. Wainwright^{*,‡}

Contribution from the Department of Chemistry, University of Adelaide, Adelaide, SA 5005, Australia, and Department of Chemistry, The Flinders University of South Australia, GPO Box 2100, Adelaide 5001, Australia

Received September 25, 1997

Abstract: ¹³C NMR studies are consistent with Δ -1,4,7,10-tetrakis((*R*)-2-hydroxy-2-phenylethyl)-1,4,7,10-tetraazacyclododecane (ΔR -thpec12) and its eight-coordinate alkali-metal complexes, $\Delta[M(R$ -thpec12)]⁺, existing predominantly as single square antiprismatic Δ diastereomers in dimethylformamide. Molecular orbital calculations show the parallel square oxygen and nitrogen planes to delineate the square antiprismatic structure of ΔR -thpec12 and $\Delta[M(R$ -thpec12)]⁺ where the basket defined by the four phenyl groups of ΔR -thpec12 becomes increasingly shallow as the M⁺ radius increases from Na⁺ to Cs⁺ and the four oxygens move further apart. An intramolecular exchange process, involving double inversion of all four nitrogen centers, occurs in ΔR -thpec12 for which $k(298.2\text{ K}) = 46300 \pm 1800\text{ s}^{-1}$, $\Delta H^\ddagger = 40.8 \pm 0.4\text{ kJ mol}^{-1}$, and $\Delta S^\ddagger = -18.8 \pm 1.7\text{ J K}^{-1}\text{ mol}^{-1}$. In $[M(R$ -thpec12)]⁺ this process is characterized by $k(298.2\text{ K}) = 233 \pm 2, 98 \pm 1, 4900 \pm 100, 33500 \pm 1000, \text{ and } 34500 \pm 1100\text{ s}^{-1}$, $\Delta H^\ddagger = 34.6 \pm 0.3, 46.1 \pm 0.2, 42.7 \pm 0.3, 39.1 \pm 0.3, \text{ and } 38.5 \pm 0.3\text{ kJ mol}^{-1}$, and $\Delta S^\ddagger = -83.5 \pm 1.1, -52.2 \pm 0.7, -31.1 \pm 1.2, -27.2 \pm 1.2, \text{ and } -28.9 \pm 1.3\text{ J K}^{-1}\text{ mol}^{-1}$, respectively, when M⁺ = Li⁺, Na⁺, K⁺, Rb⁺, and Cs⁺. For intermolecular ligand exchange on $\Delta[M(R$ -thpec12)]⁺, decomplexation is characterized by $k_d(298.2\text{ K}) = 396 \pm 3, 156 \pm 3, \text{ and } 152000 \pm 6000\text{ s}^{-1}$, $\Delta H_d^\ddagger = 46.0 \pm 0.3, 62.3 \pm 0.5, \text{ and } 69.8 \pm 0.5\text{ kJ mol}^{-1}$, and $\Delta S_d^\ddagger = -40.9 \pm 1.0, 6.0 \pm 1.9, \text{ and } 88.4 \pm 2.1\text{ J K}^{-1}\text{ mol}^{-1}$, respectively, when M⁺ = Li⁺, Na⁺, and K⁺. The stability constant, *K*, of $\Delta[M(R$ -thpec12)]⁺ varies as M⁺ changes in the sequence Li⁺ (3.13 ± 0.05), Na⁺ (4.25 ± 0.05), K⁺ (4.10 ± 0.05), Rb⁺ (3.57 ± 0.05), Cs⁺ (3.47 ± 0.05), and Ag⁺ (8.14 ± 0.03), where the figures in parentheses are log(*K*/(dm³ mol⁻¹)) determined in dimethylformamide by potentiometric titration at 298.2 K and *I* = 0.05 mol dm⁻³ (NEt₄ClO₄).

Introduction

The attachment of a coordinating pendant arm to each nitrogen of 1,4,7,10-tetraazacyclododecane results in ligands which form chiral eight-coordinate alkali-metal complex ions. Thus, achiral thec12 and tmec12 (Figure 1) form Λ and Δ enantiomeric complex ions in which chirality arises from the left- and right-handedness of the arrangement of the pendant arms in the enantiomeric square antiprismatic structures.^{1–3} Chiral 1,4,7,10-tetrakis((*S*)-2-hydroxypropyl)-1,4,7,10-tetraazacyclododecane, *S*-thpc12 (Figure 1), can in principle form two diastereomeric square antiprismatic eight-coordinate complex ions where the methyl groups all occupy either equatorial or axial positions, the Δ and Λ diastereomers, respectively, but only the latter was detected in solution.⁴ Similarly, only the ΛS -thpc12 free ligand diastereomer, which also possesses a square antiprismatic arrangement of oxygens and nitrogens, was

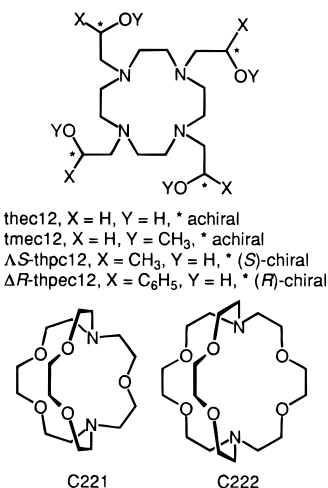


Figure 1. Ligand structures.

detected in solution. Such homochirality is unusual in macrocyclic ligands and alkali-metal complex ions, and we have now

(4) Dhillon, R. S.; Madbak, S. E.; Ciccone, F. G.; Buntine, M. A.; Lincoln, S. F.; Wainwright, K. P. *J. Am. Chem. Soc.* 1997, 119, 6126–6134.

[†] University of Adelaide.

[‡] The Flinders University of South Australia.

(1) Stephens, A. K. W.; Lincoln, S. F. *J. Chem. Soc., Dalton Trans.* 1993, 2123–2126.

(2) Whitbread, S. L.; Politis, S.; Stephens, A. K. W.; Lucas, J. B.; Dhillon, R.; Lincoln, S. F.; Wainwright, K. P. *J. Chem. Soc., Dalton Trans.* 1996, 1379–1384.

(3) Stephens, A. K. W.; Dhillon, R. S.; Madbak, S. E.; Whitbread, S. L.; Lincoln, S. F. *Inorg. Chem.* 1996, 35, 2019–2024.

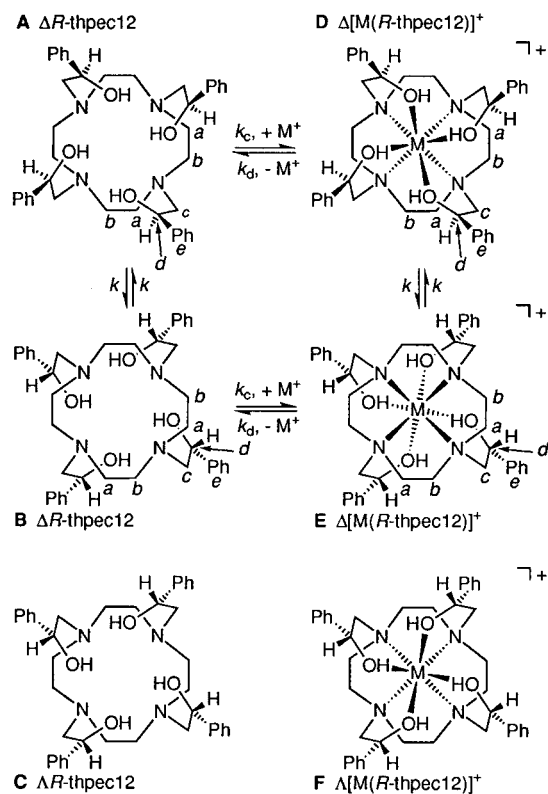


Figure 2. Exchange pathways. The Δ - and ΛR -thpec12 diastereomers are shown on the left-hand side of the figure, and the Δ - and $\Lambda[M(R$ -thpec12)]⁺ diastereomers are shown on the right-hand side of the figure.

extended our studies to Δ -1,4,7,10-tetrakis(*R*)-2-hydroxy-2-phenylethyl)-1,4,7,10-tetraazacyclododecane (ΔR -thpec12 in Figure 1) to further explore the effect of chiral pendant arms on the overall chirality of macrocyclic ligands and their alkali-metal complex ions. Our solution ¹³C NMR studies and molecular orbital calculations are consistent with ΔR -thpec12 existing predominantly as a single Δ diastereomer where the four nitrogens and the four oxygens are at the corners of the opposed parallel square faces of a square antiprism and exchange of the macrocyclic ring $-\text{CH}_2-$ between two different environments occurs through double inversion of all four nitrogen centers (Figure 2A,B). The same phenomenon is observed for the $\Delta[M(R$ -thpec12)]⁺ alkali-metal complex ions (Figure 2D,E). Thus, ΔR -thpec12 possesses a preformed cavity and may be viewed as a preorganized, but more flexible, complexing agent akin to the macrobicyclic cryptands, C221 and C222 (Figure 1), which possess relatively rigid preformed cavities.^{5,6}

Experimental Section

Δ -1,4,7,10-Tetrakis(*R*)-2-hydroxy-2-phenylethyl)-1,4,7,10-tetraazacyclododecane (ΔR -thpec12) was prepared by adding (*R*)-styrene oxide (5.06 g, 42.1 mmol, Aldrich) to a solution of 1,4,7,10-tetraazacyclododecane (1.77 g, 10.3 mmol) in dry dimethylformamide (15 cm³), and the solution was refluxed for 5 h. The solvent was removed under reduced pressure. The resulting oil was dissolved in the minimum amount of boiling 95% ethanol (ca. 20 cm³) and the solution cooled to room temperature. The white crystalline product which precipitated was filtered off and washed with cold ethanol (3 × 5 cm³). Yield: (4.1 g, 61%). Mp: 194–196 °C. Anal. Calcd for C₄₀H₅₂N₄O₄: C, 73.59; H, 8.03; N, 8.58. Found: C, 73.8; H, 8.2; N, 8.7. ¹³C NMR (CDCl₃, 295 K): δ 142.2 (4C), 128.2 (8C), 127.1 (4C), 125.9 (8C),

69.8 (4C), 64.9 (4C), 51.7 (8C). Alternatively, when (*R*)-styrene oxide (5.06 g, 42.1 mmol, Aldrich) was added to a solution of 1,4,7,10-tetraazacyclododecane (1.77 g, 10.3 mmol) in dry ethanol (15 cm³) and refluxed for 72 h, ΔR -thpec12 precipitated as colorless prisms. After cooling, ΔR -thpec12 was filtered off, washed once with cold ethanol (5 cm³), and dried in vacuo. Yield: 2.5 g (37%). 1,4,7,10-Tetraazacyclododecane (cyclen) was prepared by a literature method.⁷ The sources of the alkali-metal, silver, and tetraethylammonium perchlorates were as previously described.^{2,3} KCF₃SO₃ and its Rb⁺ and Cs⁺ analogues were prepared by reacting the stoichiometric amounts of the metal carbonates (BDH) and CF₃SO₃H (Fluka) in water and twice recrystallizing the product from water. All salts were vacuum-dried at 353–363 K for 48 h, and were stored over P₂O₅ under vacuum. (**CAUTION:** Anhydrous perchlorate salts are powerful oxidants and should be handled with care.)

Dimethylformamide was the chosen solvent because ΔR -thpec12 and its complex ions were insufficiently soluble in other common solvents for our studies. It was purified and dried by literature methods,⁸ and stored over Linde 3 Å molecular sieves under nitrogen. Its water content was below the Karl Fischer detection level of ~50 ppm. Dimethylformamide-*d*₇ (99.5% ²H) and chloroform-*d* (99.8% ²H, Aldrich) were used as received. Solutions of ΔR -thpec12 and anhydrous metal perchlorates (or triflates in the cases of K⁺, Rb⁺, and Cs⁺ for ¹³C NMR studies as the corresponding perchlorates were insufficiently soluble to give reasonable resonance intensities) were prepared under dry nitrogen in a glovebox. For the ⁷Li experiments, dimethylformamide solutions were degassed and sealed under vacuum in 5-mm NMR tubes coaxially mounted in 10-mm NMR tubes containing either acetone-*d*₆ or D₂O to provide the lock signal. For ¹³C NMR studies, dimethylformamide-*d*₇ and chloroform-*d* solutions of ΔR -thpec12 alone or with the appropriate alkali-metal salt were transferred to tightly stoppered 5-mm NMR tubes. The stabilities of $\Delta[M(R$ -thpec12)]⁺ were sufficiently high for $[\Delta[M(R$ -thpec12)]⁺] and free [M⁺] and $[\Delta R$ -thpec12] in the solutions used in the NMR studies to be those arising from the stoichiometric complexation of M⁺ by ΔR -thpec12.

Stability constants, *K*, were determined by triplicated potentiometric titrations using methods similar to those described in the literature.^{9,10} ⁷Li and ¹³C (broad-band ¹H decoupled) were run at 116.59 and 75.47 MHz, respectively, on a Bruker CXP-300 spectrometer. In the ⁷Li experiments 1000–6000 transients were collected in a 8192 database over a 1000-Hz spectral width, and for the ¹³C experiments 6000 transients were accumulated in a 8192 data point base over a 3000-Hz spectral width for each solution prior to Fourier transformation. Solution temperature was controlled to within ±0.3 K using a Bruker B-VT 1000 temperature controller. The Fourier-transformed spectra were subjected to complete line shape analysis¹¹ on a VAX 11-780 computer to obtain rate data. The temperature dependent ⁷Li and ¹³C line widths and chemical shifts employed in the complete line shape analysis were obtained by extrapolation from low temperatures where no exchange-induced modification occurred. Molecular orbital calculations were carried out using Gaussian 94 with the LanL2DZ basis set¹² on a Silicon Graphics Power Challenge and a Silicon Graphics Indigo² workstation. These calculations incorporated all electrons for H, C,

(7) Richman, J. E.; Atkins, T. J. *J. Am. Chem. Soc.* **1974**, *96*, 2268–2270.

(8) Perrin, D. D.; Armarego, W. L. F.; Perrin, D. R. *Purification of Laboratory Chemicals*, 2nd ed.; Pergamon: Oxford, 1980.

(9) Cox, B. G.; Schneider, H.; Stroka, J. J. *J. Am. Chem. Soc.* **1978**, *100*, 4746–4749.

(10) Cox, B. G.; Garcia-Rosas, J.; Schneider, H. *J. Am. Chem. Soc.* **1981**, *103*, 1384–1389.

(11) Lincoln, S. F. *Prog. React. Kinet.* **1977**, *9*, 1–91.

(12) Gaussian 94, Revision D. 3: Frisch, M. J.; Trucks, G. W.; Schlegel, H. B.; Gill, P. M. W.; Johnson, B. G.; Robb, M. A.; Cheeseman, J. R.; Keith, T.; Petersson, G. A.; Montgomery, J. A.; Raghavachari, K.; Al-Laham, M. A.; Zakrzewski, V. G.; Ortiz, J. V.; Foresman, J. B.; Cioslowski, J.; Stefanov, B. B.; Nanayakkara, A.; Challacombe, M.; Peng, C. Y.; Ayala, P. Y.; Chen, W.; Wong, M. W.; Andres, J. L.; Replogle, E. S.; Gomperts, R.; Martin, R. L.; Fox, D. J.; Binkley, J. S.; Defrees, D. J.; Baker, J.; Stewart, J. P.; Head-Gordon, M.; Gonzalez, C.; Pople, J. A.; Gaussian, Inc., Pittsburgh, PA, 1995.

(5) (a) Lehn, J.-M.; Sauvage, J. P. *J. Am. Chem. Soc.* **1975**, *97*, 6700–6707. (b) Lehn, J.-M. *Acc. Chem. Res.* **1978**, *11*, 49–57.

(6) Lehn, J.-M. *J. Inclusion Phenom.* **1988**, *6*, 351–397.

Table 1. Complex Ion Stabilities in Dimethylformamide at 298.2 K and $I = 0.05 \text{ mol dm}^{-3}$ (NEt_4ClO_4)

complex	$\log(K/(\text{dm}^3 \text{ mol}^{-1}))$					
	$\text{M}^+ = \text{Li}^+$	$\text{M}^+ = \text{Na}^+$	$\text{M}^+ = \text{K}^+$	$\text{M}^+ = \text{Rb}^+$	$\text{M}^+ = \text{Cs}^+$	$\text{M}^+ = \text{Ag}^+$
$\Delta[\text{M}(\text{R-thpec12})]^+$ ^a	3.13	4.25	4.10	3.57	3.47	8.14
$\Lambda[\text{M}(\text{S-thpec12})]^+$ ^b	3.24	3.76	3.63	3.56	3.41	11.3
$[\text{M}(\text{tmec12})]^+$ ^c	3.61	5.68	3.62	2.73	2.28	13.73
$[\text{M}(\text{thec12})]^+$ ^d	2.99	3.37	1.59	1.39	1.23	11.16
$[\text{M}(\text{C221})]^+$ ^e	3.58	7.93	6.66	5.35	3.61	12.41
$[\text{M}(\text{C222})]^+$ ^e		6.17	7.98	6.78	2.16	10.07

^a This work. Errors of ± 0.05 and ± 0.03 apply to the alkali-metal and Ag^+ complex ions, respectively, and represent 1 standard deviation. ^b Reference 4. ^c Reference 3. ^d Reference 2. ^e Reference 5.

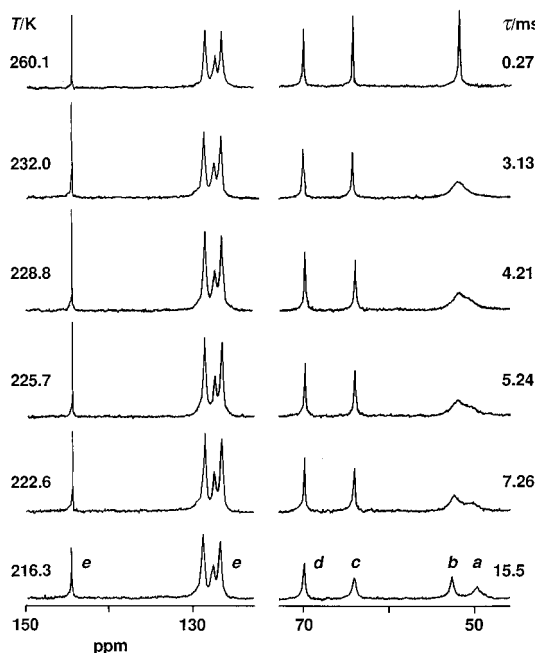


Figure 3. Temperature variation of the broad-band ^1H -decoupled ^{13}C NMR spectrum (75.47 MHz) of 0.10 mol dm^{-3} $\Delta\text{R-thpec12}$ in dimethylformamide- d_7 . Experimental temperatures and τ values derived from complete line shape analyses of the coalescing doublet arising from the macrocyclic ring carbons, *a* and *b*, appear to the left and right of the figure, respectively. The resonances arising from the pendant arm $>\text{NCH}_2-$ (*c*), $-\text{CH}(\text{C}_6\text{H}_5)\text{OH}$ (*d*), and $-\text{CH}(\text{C}_6\text{H}_5)\text{OH}$ (*e*) carbons are indicated by italic letters.

N, and O, and the valence electrons for the alkali-metal ions together with their effective core potentials.¹³

Results and Discussion

$\Delta[\text{M}(\text{R-thpec12})]^+$ Stability. The stability constant, $K = [\Delta[\text{M}(\text{R-thpec12})]^+]/[\text{M}^+][\Delta\text{R-thpec12}]$, varies with M^+ in the sequence $\text{Li}^+ < \text{Na}^+ > \text{K}^+ > \text{Rb}^+ > \text{Cs}^+$ (Table 1). (The free ligand and the complex ion diastereomer identification is discussed below.) In earlier studies, the stabilities of the closely related $[\text{M}(\text{thec12})]^+$ and $[\text{M}(\text{tmec12})]^+$ varied with M^+ and solvent consistent with their stabilities being dominated by (i) the solvation energy of M^+ , (ii) the electron-donating power of the donor atoms of thec12 and tmec12, and (iii) the ability of thec12 and tmec12 to assume a conformation that optimizes bonding with M^+ . It is probable that these three factors are the major determinants of stability for $\Delta[\text{M}(\text{R-thpec12})]^+$ also,

(13) (a) Wadt, W. R.; Hay, P. J. *J. Chem. Phys.* **1985**, *82*, 284–298. (b) Hay, P. J.; Wadt, W. R. *J. Chem. Phys.* **1985**, *82*, 299–310.

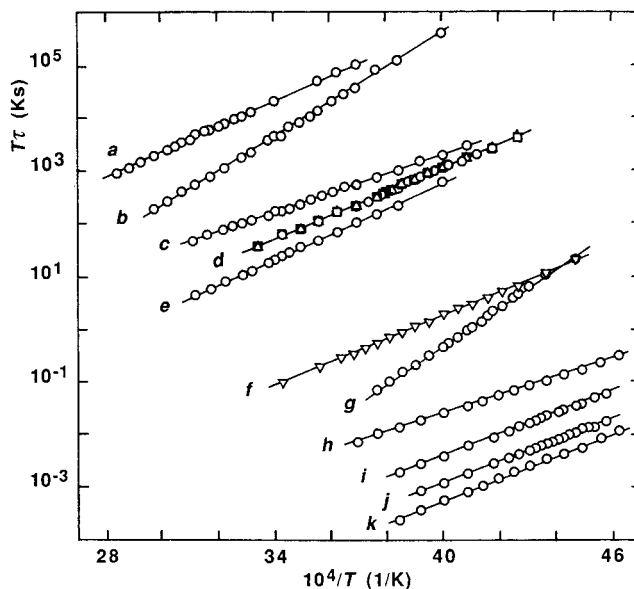


Figure 4. Temperature variations of τ for the $\Delta\text{R-thpec12}/\Delta[\text{M}(\text{R-thpec12})]^+$ systems in dimethylformamide. (a) Diastereomer exchange of $\Delta[\text{Na}(\text{R-thpec12})]^+$, 5000τ . (b) Intermolecular $\Delta\text{R-thpec12}$ exchange on $\Delta[\text{Na}(\text{R-thpec12})]^+$, 1500τ . (c) Diastereomer exchange of $\Delta[\text{Li}(\text{R-thpec12})]^+$, 100τ . (d) Intermolecular Li^+ exchange on $\Delta[\text{Li}(\text{R-thpec12})]^+$, 50τ . Data for the solutions in which the equilibrium $[\text{Li}^+]$ and $[\Delta\text{Li}(\text{R-thpec12})^+]$ were, respectively, 0.0071 and 0.0130, 0.0125 and 0.0110, and 0.0132 and 0.0069 mol dm^{-3} are represented by circles, diamonds, and squares, respectively. (e) Intermolecular $\Delta\text{R-thpec12}$ exchange on $\Delta[\text{Li}(\text{R-thpec12})]^+$, 20τ . (f) Diastereomer exchange of $\Delta[\text{K}(\text{R-thpec12})]^+$, τ . (g) Intermolecular $\Delta\text{R-thpec12}$ exchange of $\Delta[\text{K}(\text{R-thpec12})]^+$, τ . (h) Diastereomer exchange of $\Delta\text{R-thpec12}$ in chloroform- d , $\tau/10$. (i) Diastereomer exchange of $\Delta[\text{Rb}(\text{R-thpec12})]^+$, $\tau/50$. (j) Diastereomer exchange of $\Delta[\text{Cs}(\text{R-thpec12})]^+$, $\tau/150$. (k) Diastereomer exchange of $\Delta\text{R-thpec12}$, $\tau/300$. The concentrations of $\Delta\text{R-thpec12}$ alone in (h) and (k), its alkali-metal complex ion alone in (a), (c), (f), (i), and (j), and each of $\Delta\text{R-thpec12}$ and its alkali metal complex ion in (b), (d), and (e) were 0.10 mol dm^{-3} . The solid lines represent the best fits of the combined data for each group of solutions to either eq 1 or its analogue.

and that variations of their relative importance dominate the differences in stabilities among the series of alkali-metal complex ions formed by the four tetraaza macrocyclic pendant arm ligands in Table 1. The much higher stabilities of $\Delta[\text{Ag}(\text{R-thpec12})]^+$ and its analogues by comparison with their alkali-metal analogues, arise from the strong affinity of soft acid¹⁴ Ag^+ for nitrogen donor atoms.^{15,16}

These data contrast with those for the cryptates formed by 4,7,13,16,21-pentaoxa-1,10-diazabicyclo[8.8.5]tricosane, $[\text{M}(\text{C221})]^+$, for which stability also is at a maximum when $\text{M}^+ = \text{Na}^+$ (Table 1). The relatively rigid cavity radius of C221 (110 pm)⁶ more closely approximates the radius of seven-coordinate Na^+ (112 pm)¹⁷ than those of the other M^+ . This confers the highest stabilities on $[\text{Na}(\text{C221})]^+$ while the flexibility of $\Delta\text{R-thpec12}$ results in lower selectivities and stabilities for $\Delta[\text{M}(\text{R-thpec12})]^+$ where M^+ is eight-coordinate. The 140-pm cavity radius of C222 most closely approximates that of eight-coordinate K^+ (155 pm), and $[\text{K}(\text{C222})]^+$ is the most stable cryptate in the series.

(14) (a) Pearson, R. G. *J. Am. Chem. Soc.* **1963**, *85*, 3533–3539. (b) Pearson, R. G. *Coord. Chem. Rev.* **1990**, *100*, 403–425.

(15) Cotton, F. A., Wilkinson, G. *Advanced Inorganic Chemistry*, 5th ed.; Interscience: New York, 1988.

(16) Buschmann, H.-J. *Inorg. Chim. Acta* **1985**, *102*, 95–98.

(17) Shannon, R. D. *Acta Crystallogr., Sect. A: Cryst. Phys., Diffraction, Theor. Gen. Crystallogr.* **1976**, *A32*, 751–767.

Table 2. Parameters^a for Diastereomer Exchange and Intermolecular Ligand and Li⁺ Exchange in Dimethylformamide

species	<i>k</i> (298.2 K) (s ⁻¹)	ΔH^\ddagger (kJ mol ⁻¹)	ΔS^\ddagger (J K ⁻¹ mol ⁻¹)	<i>k_d</i> (298.2 K) (s ⁻¹)	ΔH_{d^\ddagger} (kJ mol ⁻¹)	ΔS_{d^\ddagger} (J K ⁻¹ mol ⁻¹)	10 ⁻⁵ <i>k_c</i> (298.2 K) (dm ³ mol ⁻¹ s ⁻¹)
ΔR -thpec12	46300 ± 1800 ^b	40.8 ± 0.4	-18.8 ± 1.7				
ΔR -thpec12 ^c	16400 ± 400 ^d	33.1 ± 0.2	-53.2 ± 1.1				
$\Delta[\text{Li}(R\text{-thpec12})]^+$	233 ± 2 ^e	34.6 ± 0.3	-83.5 ± 1.1	396 ± 3 ^f	46.0 ± 0.3	-40.9 ± 1.0	5.35
				391 ± 12 ^g	42.6 ± 0.5	-52.3 ± 2.1	5.27
$\Delta[\text{Na}(R\text{-thpec12})]^+$	98 ± 1 ^h	46.1 ± 0.2	-52.2 ± 0.7	156 ± 3 ⁱ	62.3 ± 0.5	6.0 ± 1.9	27.7
$\Delta[\text{K}(R\text{-thpec12})]^+$	4900 ± 100 ^j	42.7 ± 0.3	-31.1 ± 1.2	152000 ± 6000 ^k	69.8 ± 0.5	88.4 ± 2.1	47.2
$\Delta[\text{Rb}(R\text{-thpec12})]^+$	33500 ± 1000 ^l	39.1 ± 0.3	-27.2 ± 1.2				
$\Delta[\text{Cs}(R\text{-thpec12})]^+$	34500 ± 1100 ^m	38.5 ± 0.3	-28.9 ± 1.3				

^a Errors represent 1 standard deviation. ^b Rate constant at coalescence temperature shown in parentheses, *k*_{coal} = 241 ± 3 s⁻¹ (228.8 K). ^c In CDCl₃. ^d *k*_{coal} = 266 ± 3 s⁻¹ (320.1 K). ^e *k*_{coal} = 184 ± 2 s⁻¹ (293.5 K). ^f *k*_{coal} = 290 ± 2 s⁻¹ (293.5 K). ^g ⁷Li NMR, *k*_{coal} = 27.5 ± 0.5 s⁻¹ (260.1 K). ^h *k*_{coal} = 276 ± 2 s⁻¹ (314.8 K). ⁱ *k*_{coal} = 112 ± 2 s⁻¹ (294.5 K). ^j *k*_{coal} = 245 ± 2 s⁻¹ (256.0 K). ^k *k*_{coal} = 139 ± 1 s⁻¹ (240.3 K). ^l *k*_{coal} = 238 ± 2 s⁻¹ (229.9 K). ^m *k*_{coal} = 239 ± 2 s⁻¹ (228.8 K).

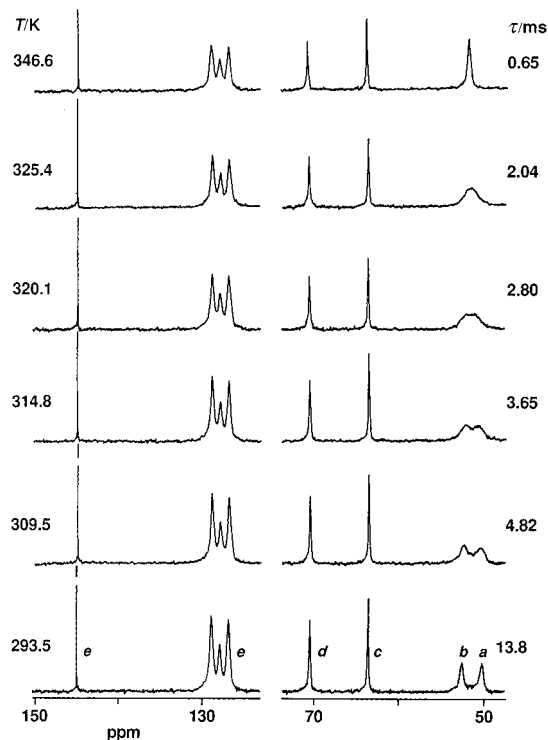


Figure 5. Temperature variation of the broad-band ¹H-decoupled ¹³C NMR spectrum (75.47 MHz) of $\Delta[\text{Na}(R\text{-thpec12})]^+$ (0.10 mol dm⁻³) in dimethylformamide-*d*₇. Experimental temperatures and τ values derived from complete line shape analyses of the coalescing doublet arising from the macrocyclic ring carbons, a and b, appear to the left and right of the figure, respectively. The resonances arising from the pendant arm >NCH₂- (c), -CH(C₆H₅)OH (d), and -CH(C₆H₅)OH (e) carbons are indicated by italic letters.

Diastereomer Exchange in ΔR -thpec12. The broad-band ¹H-decoupled ¹³C NMR spectrum of ΔR -thpec12 in dimethylformamide-*d*₇ consists of a set of eight resonances (Figure 3) under slow exchange conditions on the NMR time scale. This is consistent with a single diastereomer, identified as ΔR -thpec12 below, being present at detectable concentrations. At 216.3 K, the macrocyclic ring -CH₂- singlet resonances a and b are observed at 49.65 and 52.46 ppm, the pendant arm >NCH₂- resonance c is observed at 63.9, the -CH(C₆H₅)OH resonance d is observed at 69.83 ppm, and the -CH(C₆H₅)OH resonances e are observed at 126.70, 127.51, 128.67, and 144.36 ppm. (In chloroform-*d*, the analogous frequencies at 216.3 K are 49.62, 51.91, 64.80, 69.60, 126.07, 127.40, 128.47, and 142.03 ppm.) As the temperature increases, the pendant arm resonances c-e narrow consistent with a decrease in solution viscosity while the macrocyclic ring resonances coalesce to a singlet consistent

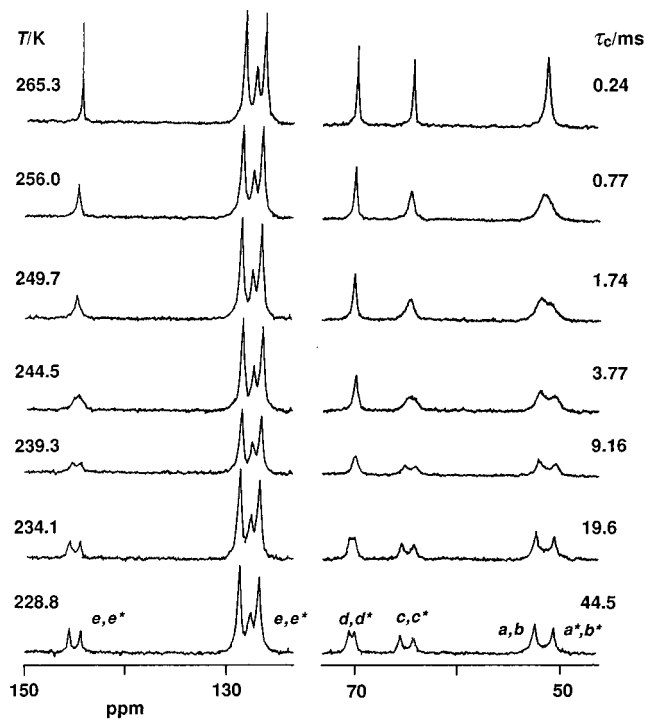


Figure 6. Temperature variation of the broad-band ¹H-decoupled 75.47-MHz ¹³C NMR spectrum of ΔR -thpec12 (0.10 mol dm⁻³) and $\Delta[\text{K}(R\text{-thpec12})]\text{CF}_3\text{SO}_3$ (0.10 mol dm⁻³), respectively, in dimethylformamide-*d*₇. Experimental temperatures and derived τ_c values appear to the left and right of the figure, respectively. At 228.8 K the resonances are assigned to the macrocyclic ring carbons of ΔR -thpec12, a* and b*, and $\Delta[\text{K}(R\text{-thpec12})]^+$, a and b, ΔR -thpec12 >NCH₂-, c*, $\Delta[\text{K}(R\text{-thpec12})]^+$ >NCH₂-, c, ΔR -thpec12 -CH(C₆H₅)OH, d*, $\Delta[\text{K}(R\text{-thpec12})]^+$ -CH(C₆H₅)OH, d, ΔR -thpec12 -CH(C₆H₅)OH, e*, and $\Delta[\text{K}(R\text{-thpec12})]^+$ -CH(C₆H₅)OH, e, for the two downfield resonances, but the other three resonances are not resolved.

with an intramolecular exchange of the macrocyclic -CH₂- between two magnetic environments, a and b, entering the fast exchange regime. Complete line shape analysis¹¹ of the coalescence of the macrocyclic -CH₂- resonances a and b yields the mean site lifetimes, τ , plotted in Figure 4 and the rate parameters, derived through eq 1, in Table 2. The >NCH₂-, -CH(C₆H₅)OH, and -CH(C₆H₅)OH resonances (c, d, and e, respectively) are not affected by this exchange process.

$$k = 1/\tau = (k_B T/h) \exp(-\Delta H^\ddagger/RT + \Delta S^\ddagger/R) \quad (1)$$

The intramolecular exchange process shown for the square antiprismatic conformation of the ΔR -thpec12 diastereomer shown in Figure 2A,B satisfies the requirements of the ¹³C NMR

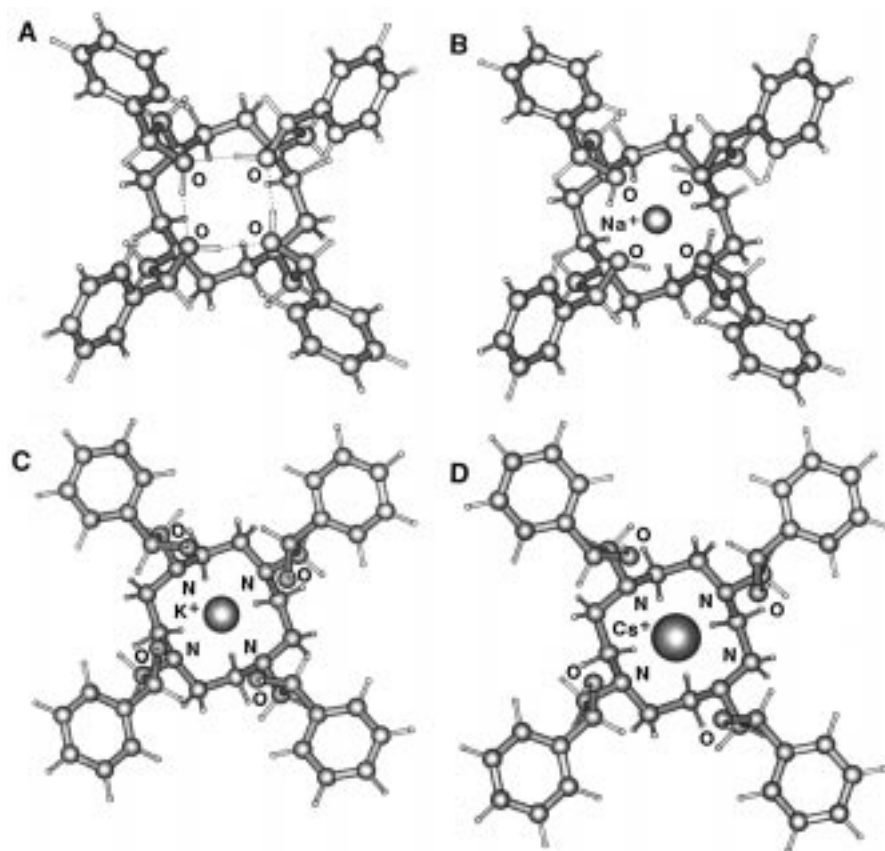


Figure 7. View approximately down the C_4 axes of the global energy-minimized structures of ΔR -thpec12 (A) and $\Delta[\text{Na}(R\text{-thpec12})]^+$ (B) and the K^+ and Cs^+ analogues (C and D) determined through Gaussian 94 using the LanL2DZ basis set. In the first two structures the oxygens mask the nitrogens. Hydrogen bonds are shown as broken lines in (A), and bonds to Na^+ , K^+ , and Cs^+ are not shown in (B), (C), and (D).

spectral temperature variation. This is readily understood if the square plane delineated by the four nitrogens is considered fixed. Thus, ΔR -thpec12 has the square plane delineated by the four hydroxy groups *above* that delineated by the four nitrogens, and two environments, *a* and *b*, exist for the macrocyclic $-\text{CH}_2-$. Double inversion about all four nitrogens produces ΔR -thpec12 (Figure 2B) in which the square plane delineated by the four hydroxy groups is *below* that delineated by the four nitrogens and exchanges the macrocyclic $-\text{CH}_2-$ between environments *a* and *b* while the pendant arms exchange between identical environments, *c-e*. If exchange between ΔR -thpec12 (Figure 2A,B) and the ΛR -thpec12 (Figure 2C) alternative diastereomer occurred, the Δ and Λ diastereomers should each exhibit eight distinct ^{13}C resonances in the slow exchange regime. Similar observations were made in chloroform-*d* consistent with ΔR -thpec12 being the only diastereomer present at detectable levels. The intramolecular exchange parameters appear in Table 2.

Diastereomer Exchange in $\Delta[\text{M}(R\text{-thpec12})]^+$. The broadband ^1H -decoupled ^{13}C NMR spectrum of $\Delta[\text{Na}(R\text{-thpec12})]^+$ in dimethylformamide-*d*₇ exhibits a temperature variation (Figure 5) consistent with the occurrence of a diastereomer exchange process similar to that observed for ΔR -thpec12, but occurring at a slower rate. Under slow exchange conditions at 216.3 K, the macrocyclic ring $-\text{CH}_2-$ singlet resonances *a* and *b* are observed at 49.45 and 52.20 ppm, pendant arm $>\text{NCH}_2-$ (*c*) and $-\text{CH}(\text{C}_6\text{H}_5)\text{OH}$ (*d*) resonances are observed at 63.16 and 69.76 ppm, respectively, and the $-\text{CH}(\text{C}_6\text{H}_5)\text{OH}$ (*e*) resonances are observed at 126.55, 127.55, 128.57, and 145.02 ppm. Similar assignments are made for the resonances observed at 216.3 K for $\Delta[\text{Li}(R\text{-thpec12})]^+$ at 49.57, 51.31, 61.91, 69.42, 126.44, 127.63, 128.63, and 144.68 ppm, for $\Delta[\text{K}(R\text{-thpec12})]^+$

at 50.31, 52.32, 65.49, 70.30, 126.67, 127.54, 128.60, and 145.44 ppm, for $\Delta[\text{Rb}(R\text{-thpec12})]^+$ at 49.98, 52.60, 63.90, 69.79, 126.62, 127.80, 128.68, and 144.33 ppm, and for $\Delta[\text{Cs}(R\text{-thpec12})]^+$ at 49.69, 52.54, 64.02, 69.81, 126.62, 127.80, 128.66, and 144.33 ppm.

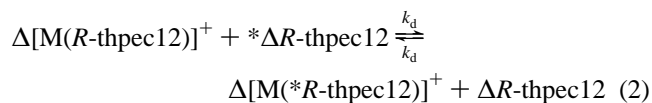
The pendant arm resonances of $\Delta[\text{Na}(R\text{-thpec12})]^+$, *c-e*, narrow slightly with an increase in temperature consistent with a decrease in solution viscosity while the macrocyclic ring resonances *a* and *b* coalesce to a singlet consistent with an intramolecular exchange of the macrocyclic $-\text{CH}_2-$ between two magnetic environments entering the fast exchange regime (Figure 5). Complete line shape analysis of the coalescence of the macrocyclic $-\text{CH}_2-$ resonances *a* and *b* yields the mean site lifetimes, τ , plotted in Figure 3 and the rate parameters in Table 2 which were derived through eq 1. The $>\text{NCH}_2-$, $-\text{CH}(\text{C}_6\text{H}_5)\text{OH}$, and $-\text{CH}(\text{C}_6\text{H}_5)\text{OH}$ resonances *c*, *d*, and *e*, respectively, are not affected by this exchange process. The spectra of the other four $\Delta[\text{M}(R\text{-thpec12})]^+$ show similar temperature dependences, but over different temperature ranges, consistent with the occurrence of exchange processes similar to that occurring in $\Delta[\text{Na}(R\text{-thpec12})]^+$.

The diastereomer exchange process proposed for $\Delta[\text{M}(R\text{-thpec12})]^+$ (Figure 2D,E) is consistent with the observed ^{13}C NMR spectral temperature variations. Thus, $\Delta[\text{M}(R\text{-thpec12})]^+$ has the square plane delineated by the four hydroxy groups *above* that delineated by the four nitrogens, and two environments, *a* and *b*, exist for the macrocyclic $-\text{CH}_2-$ (Figure 2D). Double inversion about all four nitrogens produces $\Delta[\text{M}(R\text{-thpec12})]^+$ (Figure 2E) in which the square plane delineated by the four hydroxy groups is *below* that delineated by the four nitrogens and exchanges the macrocyclic $-\text{CH}_2-$ between environments *a* and *b* while the pendant arms exchange between

identical environments, *c-e*. If exchange between $\Delta[M(R\text{-thpec12})]^+$ (Figure 2D,E) and the alternative diastereomer, $\Lambda[M(R\text{-thpec12})]^+$ (Figure 2F), occurred, each diastereomer should exhibit eight distinct ^{13}C resonances in the slow exchange regime. The observation of only one set of eight resonances is consistent with $\Delta[M(R\text{-thpec12})]^+$ alone existing at detectable concentrations.

Nitrogen double inversion in $\Delta[\text{Li}(R\text{-thpec12})]^+$ and its Na^+ and K^+ analogues is greatly slowed by comparison with that in ΔR -thpec12 (Table 2) because of the large negative ΔS^\ddagger characterizing $\Delta[\text{Li}(R\text{-thpec12})]^+$ and the larger ΔH^\ddagger and more negative ΔS^\ddagger characterizing its Na^+ and K^+ analogues, compared with these parameters for ΔR -thpec12. While ΔH^\ddagger and ΔS^\ddagger for $\Delta[\text{Rb}(R\text{-thpec12})]^+$ and its Cs^+ analogue differ substantially from those for ΔR -thpec12, there is a compensation effect which causes the nitrogen double inversion rates of these three systems to be similar. Each nitrogen double inversion requires the dissociation of a $\text{M}-\text{N}$ bond, but further mechanistic detail is unclear.

Intermolecular Exchange of ΔR -thpec12 on $\Delta[M(R\text{-thpec12})]^+$. The parameters (Table 2) for intermolecular ΔR -thpec12 exchange on $\Delta[M(R\text{-thpec12})]^+$ (eq 2) were determined



from the complete line shape analyses of the temperature dependent coalescences of the $>\text{NCH}_2-$ ^{13}C resonances of free and complexed ΔR -thpec12 for $\Delta[\text{Li}(R\text{-thpec12})]^+$, and its Na^+ and K^+ analogues (Figure 6). The temperature variation of the mean lifetime of ΔR -thpec12 in $\Delta[M(R\text{-thpec12})]^+$, $\tau_c = X_c \tau_f / X_f = 1/k_d = 1/(k_c K)$ (where τ_f is the mean lifetime of ΔR -thpec12 in the free state, X_c and X_f are the corresponding mole fractions for the $\Delta[M(R\text{-thpec12})]^+$ solutions, k_d is the decomplexation rate constant, k_c is the complexation rate constant, and K is the $\Delta[M(R\text{-thpec12})]^+$ formation constant) yields the rate parameters for the decomplexation of $\Delta[M(R\text{-thpec12})]^+$ through an equation analogous to eq 1.

The combination of a smaller ΔH_d^\ddagger and a substantial negative ΔS_d^\ddagger causes k_d for $\Delta[\text{Li}(R\text{-thpec12})]^+$ to be greater than that for $\Delta[\text{Na}(R\text{-thpec12})]^+$, while the much greater k_d for $\Delta[\text{K}(R\text{-thpec12})]^+$ results from larger ΔH_d^\ddagger and ΔS_d^\ddagger values. The nonsystematic variation of k_d , ΔH_d^\ddagger , and ΔS_d^\ddagger with change in M^+ probably indicates that changes in the solvation energy of M^+ and the amount of strain induced in the transition state with a change in the size of M^+ make varying contributions to the values of the decomplexation rate parameters as M^+ varies. While the decomplexation process involves a series of steps as octadentate ΔR -thpec12 decomplexes M^+ , the present data do not permit the assignment of a particular step as rate-determining.

The second-order complexation constant, k_c , is the product of the stability constant for the encounter complex (where ΔR -thpec12 resides in the second coordination sphere in contact with the first coordination sphere of solvated M^+) formed at a rate close to diffusion control and the first-order rate constant for the subsequent rate-determining complexation step. Its variation with M^+ is 100-fold smaller than that for k_d which indicates that the decomplexation transition state more closely resembles solvated M^+ and free ΔR -thpec12 than it does $\Delta[M(R\text{-thpec12})]^+$. The activation parameters for the decomplexation of $\Delta[M(R\text{-thpec12})]^+$ and the nitrogen double inversion in $\Delta[M(R\text{-thpec12})]^+$ are significantly different, consistent with the two processes following different reaction paths.

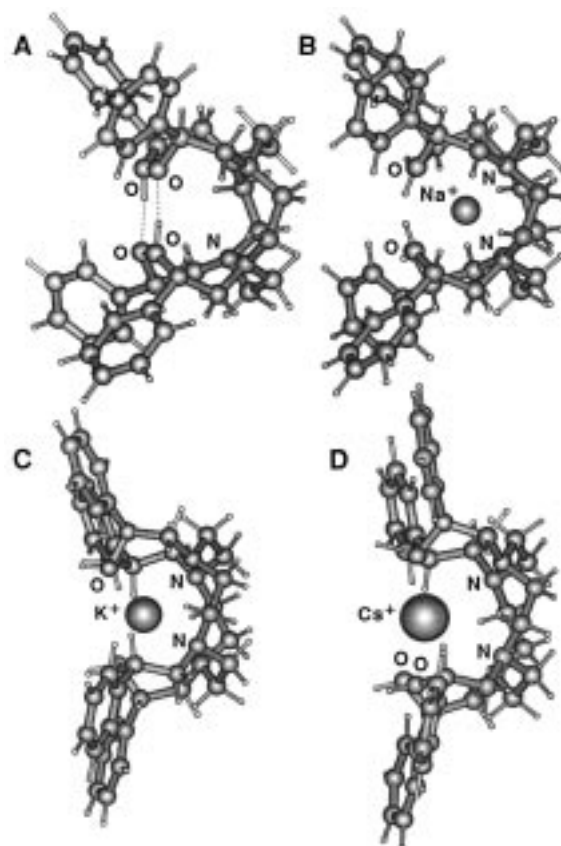


Figure 8. Side views of the global energy minimized structures of ΔR -thpec12 (A) and $\Delta[\text{Na}(R\text{-thpec12})]^+$ (B) and the K^+ and Cs^+ analogues (C and D) determined through Gaussian 94 using the LanL2DZ basis set. In all four structures either some oxygens or some nitrogens or both are masked by other atoms. Hydrogen bonds are shown as broken lines in (A), and bonds to Na^+ , K^+ , and Cs^+ are not shown in (B), (C), and (D).

Nevertheless, because $\text{M}-\text{N}$ bond breaking is necessary for the exchange between the equivalent forms of $\Delta[M(R\text{-thpec12})]^+$ to proceed, it is possible that part of this process is similar to that preceding decomplexation. Some support for this view is afforded by the observation that lability toward the first process follows the M^+ sequence $\text{K}^+ > \text{Li}^+ > \text{Na}^+$ which is the same as that for the second. Intermolecular exchange of ΔR -thpec12 in $\Delta[\text{Li}(R\text{-thpec12})]^+$ and its Na^+ analogue is moderately faster than their diastereomer exchange processes, and for the K^+ analogue it is 30 times faster. The intermolecular ligand exchange processes on $\Delta[\text{Rb}(R\text{-thpec12})]^+$ and its Cs^+ analogue were in the fast exchange regime of the ^{13}C NMR time scale at 216.3 K so that broadened environmentally averaged ^{13}C resonances were seen.

A ^7Li NMR kinetic study of the intermolecular exchange of Li^+ between the solvated state and $\Delta[\text{Li}(R\text{-thpec12})]^+$ yielded the mean lifetimes, τ , of Li^+ in $\Delta[\text{Li}(R\text{-thpec12})]^+$ from a complete line shape analysis of the coalescence of the ^7Li resonances of solvated Li^+ and $\Delta[\text{Li}(R\text{-thpec12})]^+$. These data are plotted in Figure 4 from which it is seen that τ is independent of $[\text{Li}^+_{\text{solvated}}]$, consistent with the operation of a dominant monomolecular exchange mechanism. The kinetic parameters derived from these τ data (Table 2) are similar to those for ligand exchange on $\Delta[\text{Li}(R\text{-thpec12})]^+$ derived from the ^{13}C NMR data. The resonance of $\text{Li}^+_{\text{solvated}}$ appears 0.30 ppm downfield from that of $\Delta[\text{Li}(R\text{-thpec12})]^+$ at 234.1 K, and their coalescence with an increase in temperature follows the usual pattern.⁴

Molecular Orbital Calculations. The approximately cubic global energy-minimized ΔR -thpec12 structure calculated using

Table 3. Parameters Derived from Molecular Orbital Calculations Using the Gaussian 94 LanL2DZ Basis Set^a

param	ΔR -thpec12	$\Delta[M(R\text{-thpec12})]^+$				
		$M^+ = \text{Li}^+$	$M^+ = \text{Na}^+$	$M^+ = \text{K}^+$	$M^+ = \text{Rb}^+$	$M^+ = \text{Cs}^+$
O–O distance (pm)	272	O1–O2 = 267 O2–O3 = 262 O3–O4 = 268 O4–O1 = 269	276	370	408	446
N–N distance (pm)	317	N1–N2 = 301 N2–N3 = 302 N3–N4 = 302 N4–N1 = 304	311	321	325	328
O–N distance (pm)	292	O1–N1 = 296 O2–N2 = 281 O3–N3 = 296 O4–N4 = 290	292	302	306	310
M–O distance (pm)		Li–O1 = 288 Li–O2 = 239 Li–O3 = 292 Li–O4 = 277	254	282	299	318
M–N distance (pm)		Li–N1 = 232 Li–N2 = 227 Li–N3 = 232 Li–N4 = 236	254	294	314	338
M–O plane distance (pm)		<i>b</i>	163	106	79	48
M–N plane distance (pm)		<i>c</i>	128	188	215	245
H–O distance ^d (pm)	97	97	96	95	95	95
H–O distance ^e (pm)	176	H1–O4 = 176 H2–O1 = 172 H3–O2 = 178 H4–O3 = 179	193 ^f	395 ^f	439 ^f	483 ^f
twist angle ϕ^g (deg)	3.3	<i>h</i>	2.2	5.4	2.3	1.2
angle between phenyl plane and O plane (deg) ^j	36.1	<i>j</i>	33.9	23.4	18.6	13.5

^a The globalized minimum energies for ΔR -thpec12 and its Li^+ , Na^+ , K^+ , Rb^+ , and Cs^+ complex ions are -2061.6107 , -2069.0531 , -2061.7770 , -2089.4281 , -2085.1408 , and -2081.1503 H, respectively, where 1 H = $2617.13 \text{ kJ mol}^{-1}$. ^b The oxygen atoms have no common plane. ^c The nitrogen atoms have no common plane. ^d The distance between H and O in hydroxy groups. ^e The distance between the H and O of adjacent hydroxy groups. ^f No hydrogen bonding. ^g Twist angle $\phi = 0^\circ$ for a cubic structure. ^h No meaningful ϕ as C_4 symmetry is absent. ⁱ An angle of 0° exists when the phenyl and the O planes are parallel. ^j No meaningful angle as C_4 symmetry is absent.

Gaussian 94¹² has C_4 symmetry (Figures 7A and 8A and Table 3) and shows near superimposition of the two parallel square planes delineated by four oxygens and four nitrogens, respectively. The hydroxy protons point toward the adjacent hydroxy oxygen and are at distances where weak hydrogen bonding exists.¹⁸ The (*R*)-2-hydroxy-2-phenylethyl arms are oriented in a clockwise direction when viewed down the C_4 axis from the four-oxygen plane so that the phenyl groups project out from the structure. This makes the two carbons in each macrocyclic ethylene linkage inequivalent, in broad agreement with the ΔR -thpec12 structure proposed on the basis of the ¹³C NMR studies. Each pair of ethylene carbons are equivalent to the other pairs, and a similar equivalence applies for the pendant arms.

Four basic structures with either four, three, two adjacent, or two diagonally opposed pendant arms on the same side of the tetraaza plane were selected as minimization starting points. A range of macrocyclic ring conformations were then superimposed on these structures to widen the selection of starting points. In all cases the energy-minimized structure obtained was that shown in Figures 7A and 8A, consistent with a global energy minimum being reached. Analogous starting point structures were used to test that the $\Delta[M(R\text{-thpec12})]^+$ structures shown in Figure 7 and listed in Table 3 were also global minimized structures. Selected computed interatomic distances for ΔR -thpec12 and $\Delta[M(R\text{-thpec12})]^+$ appear in Table 3.

The computed distorted cubic structure for $\Delta[\text{Na}(R\text{-thpec12})]^+$ (Figures 7B and 8B) and its K^+ (Figures 7C and 8C) and Rb^+ and Cs^+ (Figures 7D and 8D) analogues also possess C_4

symmetry and have chiral characteristics similar to those of ΔR -thpec12. However, the O–O, N–N, and O–N distances all increase with the size of the cation, M^+ , and the M–O and M–N plane distances decrease and increase, respectively, as cation size increases from Na^+ to Cs^+ . It is seen in Figures 7 and 8 that the increase in size of the cation causes the structure of coordinated ΔR -thpec12 to open out substantially. A measure of this is gained from the changing angle between the plane of the phenyl rings and the O plane which decreases markedly as cation size increases. The twist angle between the O and N planes is small and shows a nonsystematic variation. The M^+ is centrally positioned in the ligand cavity, and the (*R*)-2-hydroxyphenylethyl arms are oriented in a clockwise direction so that the phenyl groups project out from the structure and render the two carbons in each macrocyclic ethylene linkage inequivalent as found in the ¹³C NMR studies discussed above. The similarity of the $\Delta[\text{Na}(R\text{-thpec12})]^+$ and ΔR -thpec12 dimensions indicates a near optimum fit of Na^+ to the ΔR -thpec12 cavity. The computed $\Delta[\text{Li}(R\text{-thpec12})]^+$ structure does not possess C_4 symmetry as is shown by the variation in the Li–O and Li–N distances (Table 3), consistent with Li^+ being too small for an optimum fit into the ΔR -thpec12 cavity. (If the solution structure of $\Delta[\text{Li}(R\text{-thpec12})]^+$ is similar to the computed structure, it appears that a fluxional motion renders all of the four (*R*)-2-hydroxy-2-phenylethyl arms equivalent and all four macrocyclic ring ethylenic moieties equivalent in the fast exchange limit of the ¹³C NMR time scale which is much faster than the nitrogen double inversion process.) A similar lack of C_4 symmetry was reported for the closely related computed $\Delta[\text{Li}(S\text{-thpec12})]^+$ structure.⁴

The computed ΔR -thpec12 structure and the five $\Delta[M(R\text{-thpec12})]^+$ structures possess the same macrocyclic ring conformation, which is similar to that observed in the X-ray-determined crystal structures of their $[M(\text{thec12})]^+$ analogues.^{19–21} In general terms the computed structures of ΔR -thpec12 and $\Delta[M(R\text{-thpec12})]^+$ add plausibility to the interpretation of the ¹³C NMR data above in terms of single ΔR -thpec12 and $\Delta[M(R\text{-thpec12})]^+$ diastereomers.

Conclusion

Δ -1,4,7,10-Tetrakis((*R*)-2-hydroxy-2-phenylethyl)-1,4,7,10-tetraazacyclododecane (ΔR -thpec12) and its eight-coordinate alkali-metal complexes, $\Delta[M(R\text{-thpec12})]^+$, exist predominantly as single square antiprismatic Δ diastereomers (Figure 2) that undergo exchange between equivalent diastereomeric forms in dimethylformamide. The alternative ΛR -thpec12 and $\Lambda[M(R\text{-thpec12})]^+$ diastereomers appear to be less stable and were not detected. Molecular orbital calculations, which yield ΔR -

thpec12 and $\Delta[M(R\text{-thpec12})]^+$ with C_4 symmetry (except for $\Delta[\text{Li}(R\text{-thpec12})]^+$ where Li^+ is not centrally located in the ligand cavity) as global energy-minimized structures, support these deductions. The structure of the eight-coordinated ΔR -thpec12 in the computed structures opens out so that the basket-like structure delineated by the four phenyl groups becomes shallower and wider as M^+ moves away from the tetraaza plane and closer to the tetraoxa plane in the sequence Na^+ through Cs^+ . These computed structure variations coincide with an increase in the rate of exchange between equivalent $\Delta[M(R\text{-thpec12})]^+$ diastereomers in the same sequence, and a decrease in the stabilities of $\Delta[M(R\text{-thpec12})]^+$ as M^+ changes from Na^+ to Cs^+ . It is planned to test the molecular receptor characteristics of the adjustable basket-like structures of ΔR -thpec12 and $\Delta[M(R\text{-thpec12})]^+$ in future studies.

Acknowledgment. Funding of this study by the Australian Research Council, the University of Adelaide, and the Flinders University of South Australia is gratefully acknowledged, as are the computing resources provided by the South Australian Center for Parallel Computing.

JA973367L

(19) Buøen, S.; Dale, J.; Groth, P.; Krane, J. *J. Chem. Soc., Chem. Commun.* **1982**, 1172–1174.

(20) Groth, P. *Acta Chem. Scand. A* **1983**, 37, 71–74.

(21) Groth, P. *Acta Chem. Scand. A* **1983**, 37, 283–291.